Element-Specific Probing of Ultrafast Spin Dynamics in Multisublattice Magnets with Visible Light

A. R. Khorsand,[1,*] M. Savoini,[1] A. Kirilyuk,[1] A. V. Kimel,[1] A. Tsukamoto,[2,3] A. Itoh,[2] and Th. Rasing[1]

[1]*Institute for Molecules and Materials, Radboud University Nijmegen, Heyendaalseweg 135, 6525 AJ Nijmegen, The Netherlands*

[2]*College of Science and Technology, Nihon University, 7-24-1 Funabashi, Chiba, Japan*

[3]*Japan Science and Technology Agency, PRESTO, 4-1-8 Honcho Kawaguchi, Saitama, Japan*

(Received 5 July 2012; published 7 March 2013)

We demonstrate the feasibility of element-specific probing of ultrafast spin dynamics in the multisublattice magnet TbFe in the visible spectral range. In particular, we show that one can selectively study the dynamics of Tb and Fe sublattices choosing the wavelength of light below and above 610 nm, respectively. We observe that, despite their antiferromagnetic coupling in the ground state, the Tb and Fe spins temporarily align ferromagnetically after excitation with an intense 55-fs laser pulse, after which they relax to their initial states due to the strong anisotropy in Tb.

DOI: 10.1103/PhysRevLett.110.107205 PACS numbers: 75.50.Gg, 42.62.Fi, 71.70.Gm, 75.50.Ss

Femtosecond laser excitation of multisublattice magnets opens the way to trigger ultrafast spin dynamics and even magnetization reversal driven by the strong exchange interaction between the sublattices [1,2]. To explore and exploit these intriguing possibilities requires femtosecond time-resolved and element-specific studies of the spin dynamics in multisublattice systems.

The wave functions of the magnetic states in metals probed in the visible spectral range have, in general, a substantial overlap. This fact has been a serious obstacle for experimental studies of element-specific ultrafast magnetization dynamics. Until now it has been a conventionally accepted wisdom that ultrafast and element-specific probing of magnetism in the visible spectral range is hardly possible, and only photons in the soft-x-ray [2,3] and EUV [4] regimes were used for such studies probing transitions of strongly localized electrons whose exchange split energy levels serve as the fingerprint of the element.

However, techniques utilizing high-energy photons have some great limitations, in particular, in combination with subpicosecond time resolution. For instance, the number of photons per pulse is small and subject to fluctuations, giving rise to an extremely low signal-to-noise ratio and time-consuming measurements. Furthermore, the generation of soft-x-ray fs pulses requires rather unique and demanding sources, and the access to such facilities is very limited.

In this Letter, we formulate requirements which allow element-specific probing in the visible spectral range. We study ultrafast laser-induced magnetization dynamics of a TbFe alloy, and find that one can selectively study the dynamics of Tb and Fe spins choosing the wavelength of light below and above 610 nm, respectively. Furthermore, we find that at high excitation intensities the antiferromagnetically coupled spins temporarily align ferromagnetically, succeeded with magnetization recovery, in striking contrast to GdFe where the magnetization reverses.

The feasibility of element-specific spin dynamics with visible light is investigated on a TbFe-based alloy. The magnetic material is an amorphous, thin ferrimagnetic film of 20 nm. The composition is 16% Tb, 75% Fe, and 9% Co, with an out-of-plane anisotropy and a coercive field of 1 T. The magnetic moments of Tb and FeCo form two antiferromagnetically coupled sublattices with similar, though nonequivalent, magnetic moments at room temperature. In the following, we focus on the behavior of Tb and Fe and ignore the small contribution of angular momentum of Co.

Both static magneto-optic Kerr effect (MOKE) and time-resolved (TR) MOKE measurements [5–9] were performed at room temperature. We define the Kerr rotation as the difference in rotation of linearly polarized light for positive and negative magnetization, i.e., $\theta_K = \theta_{+M}\text{-}\theta_{-M}$. This ensures that θ_K is of a purely magnetic origin. In Fig. 1(a) the spectral dependence of the static Kerr rotation $\theta_{K,0}$ is shown, i.e., the Kerr rotation of TbFe in the absence of an excitation pulse. The spectrum contains three features: (i) a small but positive signal in the (infra)red regime, (ii) a sign change around 610 nm, and (iii) a large and relatively sharp peak around 500 nm.

In a material with two magnetic sublattices, the Kerr rotation consists of the collective response of both magnetic species. In an isotropic medium in a polar geometry [see inset of Fig. 2(b)], the Kerr rotation is in first order approximation given by [10,11]

$$\theta_K(\lambda) = \theta_1(\lambda) + \theta_2(\lambda) = K_1(\lambda)M_1 + K_2(\lambda)M_2, \quad (1)$$

where θ_i, M_i, and K_i are the Kerr rotation, out-of-plane component of the magnetization, and MO susceptibility of

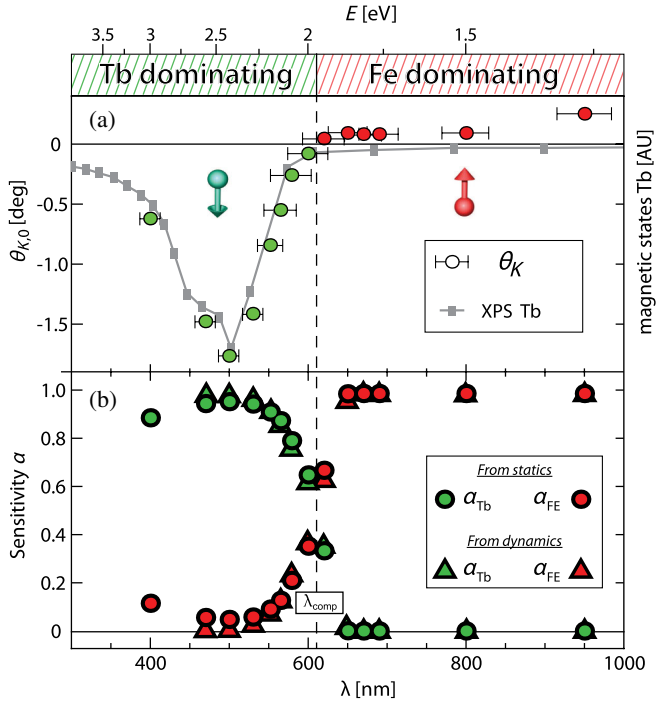

FIG. 1 (color online). Response of the TbFe alloy as a function of the probe wavelength (bottom axis) and photon energy (top axis). (a) The static Kerr rotation (dots), and the magnetic states in the $4f$ shell of Tb (solid line). The latter was measured with spin-polarized x-ray photoemission (adapted from Ref. [12]). (b) The sensitivity α to Fe (red) and Tb (green) sublattices obtained from static MOKE (dots) and TR MOKE (triangles) measurements.

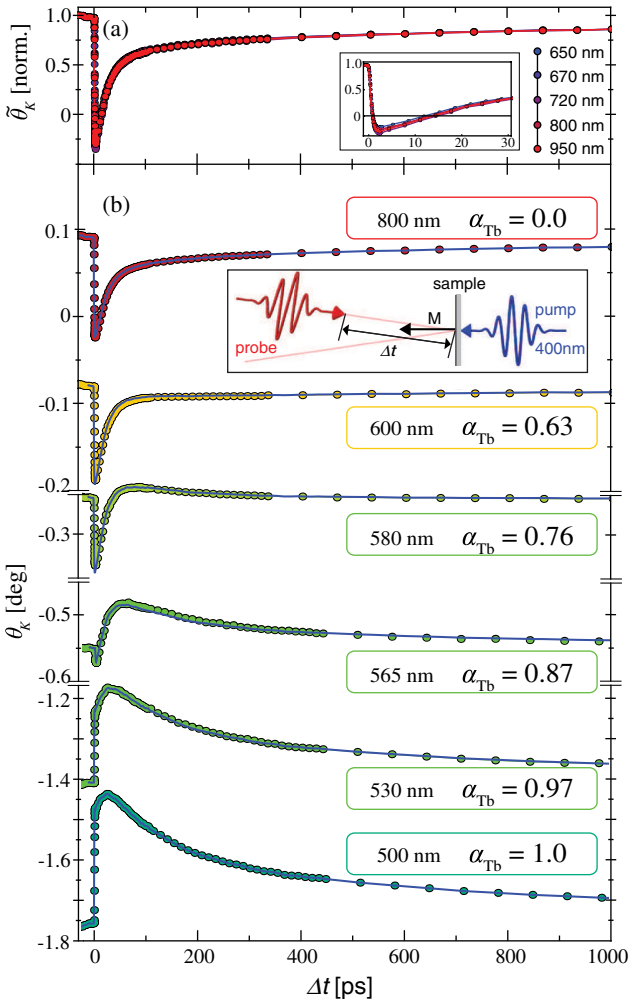

FIG. 2 (color online). Spectral dependence of TR MOKE measurements at a fixed excitation fluence of 4.4 mJ/cm^2. TR MOKE at (a) $\lambda = 650$–950 nm and (b) $\lambda = 500$–800 nm. The blue solid lines in (b) are the fits to Eq. (3), where the fitting parameters α_{Tb} are given at the right at each wavelength. Inset: Geometry of the pump-probe pulses with respect to the sample.

sublattice i, respectively. The probe sensitivity α_i to sublattice i is defined with

$$\alpha_i(\lambda) = \frac{|\theta_i(\lambda)|}{|\theta_{\mathrm{Tb}}(\lambda)| + |\theta_{\mathrm{Fe}}(\lambda)|}. \quad (2)$$

K_{Fe} and K_{Tb} have the same sign and do not reverse at $\lambda = 400$–950 nm [10,11], whereas M_{Fe} and M_{Tb} have opposite signs due to the antiferromagnetic coupling. Therefore, the Kerr rotations of the Tb and Fe sublattices are opposite to each other. When their magnitudes are equivalent, i.e., $\alpha_{\mathrm{Fe}} = \alpha_{\mathrm{Tb}} = 0.5$, the net Kerr rotation of TbFe goes to zero. This is the case around 610 nm. Above and below this wavelength, the sign of the net Kerr rotation is given by the sublattice with the dominant contribution to the MO contrast; i.e., the sublattice for which $\alpha_i > 0.5$. We identify the wavelength regimes above and below 610 nm as the Fe and Tb dominated regimes, respectively.

In magnetic transition metals (TMs) (e.g., Fe, Ni, and Co), the magnetic moment is carried by itinerant $3d$ electrons near the Fermi level (E_F). Because of the many possible low-energy transitions within the conduction band of these ferromagnets, their Kerr rotations are significant in the infrared (IR) regime. On the other hand, the largest part of the magnetic moment of rare-earth metals is carried by the localized $4f$ electrons [12–14], which is roughly 97% in Tb. The other 3% is carried by $5d$ conduction electrons. Spin-polarized XPS data of Tb are shown in Fig. 1(a) (adapted from Ref. [12]), from which we find that the $4f$ shell is around 2.4 eV below E_F. The $4f$ electrons of Tb become accessible in the visible spectral range, and also the conduction electrons are accessible at 2–3 eV [15]. This gives rise to a high Kerr rotation of the Tb sublattice in this regime. In fact, it can be seen from the XPS data in Fig. 1(a) that the large peak of the Kerr rotation around 500 nm is very closely related to the spin-polarized states of Tb, indicating that the MO response comes mainly from Tb.

The wavelength dependence of the MO response is studied in more detail with TR MOKE measurements at a fixed excitation fluence of 4.4 mJ/cm^2. First, we consider the dynamics in the regime $\lambda \geq 650$ nm shown in

Fig. 2(a). The normalized transient Kerr rotation, i.e., $\tilde{\theta}_K(\lambda, t) \equiv \frac{\theta_K(\lambda,t)}{\theta_{K,0}(\lambda)}$, is plotted as a function of the pump-probe delay time for various probe wavelengths. It can be seen that the MO response is independent of the probe wavelength, which demonstrates that the sensitivities α_{Fe} and α_{Tb} are constant at $\lambda > 650$ nm.

At shorter wavelengths, the probe is sensitive to more than one sublattice. Otherwise, the magnetization dynamics $M_i(t)/M_0$ of sublattice i would be given by $\theta_K(t)/\theta_{K,0}$, and the measurements at 565–600 nm would have the unphysical implication that the absolute value of the magnetic moment increases shortly after excitation. On the other hand, if the measurements give the collective response of two sublattices, it should be possible to reproduce all profiles from two traces, i.e., from the Tb and Fe dominated responses at 500 and 800 nm, respectively. We can examine this by fitting the dynamics measurements to the following function:

$$\theta_{\mathrm{fit}}(\lambda, t, \alpha_1) = \theta_{K,0}(\lambda)\frac{(1-\alpha_{\mathrm{Tb}})\tilde{\theta}_{\mathrm{Fe}}(t) - \alpha_{\mathrm{Tb}}\tilde{\theta}_{\mathrm{Tb}}(t)}{1-2\alpha_{\mathrm{Tb}}}, \quad (3)$$

where $\theta_{K,0}(\lambda)$ is the static Kerr rotation taken from Fig. 1(a), and $\tilde{\theta}_{\mathrm{Tb}}(t)$ and $\tilde{\theta}_{\mathrm{Fe}}(t)$ are the normalized time resolved Kerr rotations at 500 and 800 nm, respectively. The denominator $(1-2\alpha_{\mathrm{Tb}})$ ensures that the right-hand term is normalized to $+1$ at $t < 0$. We note that we use only one fitting parameter, namely, α_{Tb}, in order to fit the whole set of time dependencies at probe wavelength λ. The fits are shown in Fig. 2(b) as solid blue lines and are in excellent agreement with the measurements. This demonstrates that there are only two traces that give rise to the TR MOKE measurements at $\lambda = 500$–950 nm, and validates Eq. (1) in this wavelength range.

Having demonstrated that we can readily measure different parts of the magnetization of TbFe by changing the probe wavelength, we have a closer look at the MO responses at 500 and 800 nm. The demagnetization profiles show features which are typical for Fe and Tb. The demagnetization at 800 nm is ultrafast ($\tau \approx 0.2$ ps), succeeded by a recovery. Such "one-step demagnetization" is typical for $3d$ TMs like Fe [5–8]. On the other hand, at 500 nm the drop of the MO signal is initially ultrafast ($\tau \approx 0.4$ ps), succeeded by slow demagnetization ($\tau \approx 15$ ps) before it recovers. Such "two-step demagnetization" is typical for rare-earth metals such as Tb [7,16], and is generally assigned to their large magnetic moments. Therefore, the TR MOKE measurements at 500 and 800 nm reveal fingerprints of the Tb and Fe sublattices, respectively. This is in agreement with the static MOKE measurements shown in Fig. 1(a) from which we concluded that the probe is sensitive to dominantly the Tb and Fe sublattice at wavelengths below and above 610 nm, respectively.

Apart from a different shape of the demagnetization profile, there is a large difference in the change in the MO contrast. The maximum change of the MO contrast

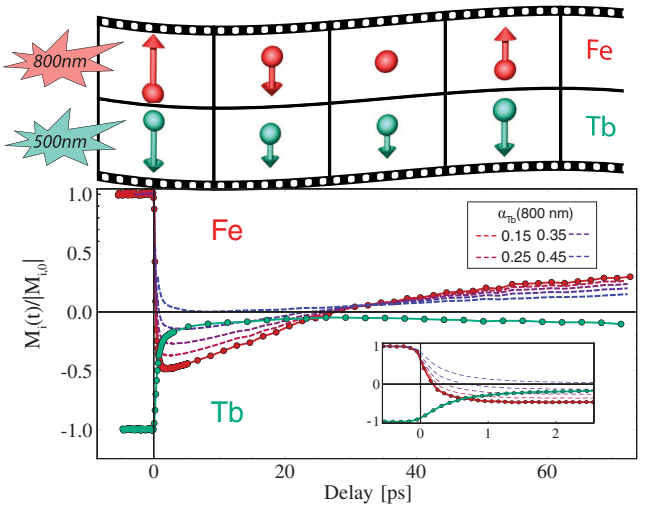

FIG. 3 (color online). Ultrafast sublattice magnetization dynamics of TbFe at $\lambda_{\mathrm{Fe}} = 800$ nm and $\lambda_{\mathrm{Tb}} = 500$, corresponding to dominantly the Fe and Tb sublattices, respectively. The excitation fluence was 8 mJ/cm^2. The dashed lines give the magnetization dynamics of Fe for various sensitivities to Tb at 800 nm.

is much smaller at 500 nm ($\approx 20\%$) compared to 800 nm ($> 100\%$). At an excitation intensity of 8 mJ/cm^2 shown in Fig. 3, these values are 95% and 150%, respectively.

The magnetization dynamics of each sublattice can be extracted from the TR MOKE measurements once the probe sensitivity to each sublattice is known at 500 and 800 nm. In general, the sublattice sensitivities at different optical wavelengths could be deduced with a calibration from x-ray magnetic circular dichroism (XMCD) measurements. This can be done by fitting one series of TR XMCD measurements at the Fe and Tb edges to TR MOKE traces at λ_1 and λ_2 measured under the same conditions, with a similar fitting as with Eq. (3). In fact, when TR MOKE measurements are combined with such calibration measurements, element-specific information could be obtained with visible light for two-sublattice magnets in general. The only condition is that the probe sensitivity to the two sublattices is different at λ_1 and λ_2 [17]. This condition is met in many alloys, such as in rare-earth-metal–transition-metal alloys but also in TM-TM alloys such as FeNi. For example, θ_K of Fe and Ni have very different spectral dependencies: at 300 nm $\theta_{K,\mathrm{Ni}} \approx 0°$ and $\theta_{K,\mathrm{Fe}} \approx 0.3°$, whereas at 400 nm $\theta_{K,\mathrm{Ni}} \approx 0.2°$, and $\theta_{K,\mathrm{Fe}} \approx 0.3°$ [18]. Once the probe sensitivities are extracted from the calibration measurements, sublattice dynamics can be studied with visible light at different conditions, such as different excitation intensities or magnetic fields. Thus, despite the calibration with high-energy photons, this procedure allows element-specific measurements with the unique advantages of an optical probe.

For TbFe, however, we can estimate the probe sensitivity to the Fe and Tb sublattices as their magnetization is

largely contained at different energy levels. We use the static MOKE and TR MOKE measurements, in combination with the fact that the Kerr rotation of pure Fe decreases only a little in the regime $\lambda < 650$ nm [18]. Using $\theta_{\mathrm{Fe}}(\lambda) \lesssim\approx 90$ mdeg, the sensitivity to the Tb sublattice at $\lambda = 400$–650 nm can be readily calculated with Eq. (2) and is shown in Fig. 1(b). We find that at 500 nm almost all signal comes from Tb, i.e., $\alpha_{\mathrm{Tb}} > 0.95$.

On the other hand, TR MOKE measurements have revealed that at longer wavelengths (650–950 nm) the sensitivities α_{Tb} and α_{Fe} are constant. In this low-energy regime, MO properties arise from transitions within the conduction band. Transition metals such as Fe have a relatively large MO susceptibility in this regime as their magnetic moments are contained within the conduction band. The Tb sublattice can also contribute to the Kerr rotation in the IR regime through the $5d$ conduction electrons which carry approximately 3% of the magnetic moment. The Kerr rotation of Tb, however, is typically very small compared to Fe. We measured the Kerr rotations of 20 nm thin Tb and Fe films at 800 nm to be $\theta_{\mathrm{Tb}} \approx 10$ mdeg (at 100 K) and $\theta_{\mathrm{Fe}} \approx 350$ mdeg, respectively. We estimate from this that the contribution of Tb to the MO signal of TbFe is negligible in the IR regime and that $\alpha_{\mathrm{Fe}} \approx 1$. The thus obtained values are shown in Fig. 1(b) and are in excellent agreement with the fitted values from the dynamics measurements in Fig. 2.

It should be noted that the relative Kerr rotations of Tb and Fe in alloys may deviate from their pure forms. Using Eq. (3), we calculated the sublattice magnetization dynamics of Fe from θ_K (t,800 nm) for $0 < \alpha_{\mathrm{Tb}} < 0.5$. It can be seen that even under the conservative assumption that $\alpha_{\mathrm{Fe}} = 0.65$ ($\alpha_{\mathrm{Tb}} = 0.35$), the TR MOKE measurement at 800 nm indicates that the magnetization of Fe temporarily reverses sign. Only in the coincidental case that the relative contribution of Tb and Fe is almost equal at 800 nm, i.e., $1 < |\theta_{\mathrm{Fe}}/\theta_{\mathrm{Tb}}| < 1.2$ ($0.45 < \alpha_{\mathrm{Tb}} < 0.5$), then the magnetization of the Fe sublattice would not reverse. We find this very unlikely as this ratio is much smaller compared to their pure forms, i.e., $|\theta_{\mathrm{Fe}}/\theta_{\mathrm{Tb}}| \approx 35$. Furthermore, a net Kerr rotation of ≈ 300 mdeg at 950 nm with $\alpha_{\mathrm{Tb}} > 0.45$ would imply that the absolute Kerr rotations of the Tb and Fe sublattices would be larger than 1.35 and 1.65 deg, respectively. Thus, correcting for the small fraction of Tb in TbFe, this would give the improbable implication that the Kerr rotation of Tb would be 3 orders of magnitude larger in this alloy compared to pure Tb.

Therefore, the reversal of the MO contrast at 800 nm is assigned to the reversal of the Fe magnetization. This reversal leads to a transient magnetic state in which both sublattices are aligned ferromagnetically, despite their antiferromagnetic coupling in the ground state. A transient ferromagnetic state was recently observed in GdFeCo [2], which has an antiferromagnetic coupling in its ground state, too. It was demonstrated that such a transient ferromagnetic magnetic state is a necessary and sufficient condition for all-optical magnetization reversal in GdFeCo [2,19]; i.e., the reversal of both magnetic sublattices with a single laser pulse [1,20]. In TbFeCo, however, we observe a different behavior; the transient ferromagnetic state is succeeded by the recovery of the magnetization.

The striking difference in the dynamics of TbFeCo and GdFeCo may be explained by the large difference in spin-orbit coupling in the two rare-earth-metal materials. Gadolinium has an exactly half-filled $4f$ shell. Therefore, its net orbital moment is zero and the spin-orbit coupling is very weak. As a consequence, the spins of the Gd atoms are coupled only weakly to the lattice, allowing them to follow the Fe spins relatively easily. Terbium, on the other hand, is known for its strong spin-orbit coupling. Therefore, Tb spins are not only coupled to the spins of the Fe sublattice, but also to the lattice. This leads to two competing forces acting on the Tb spins. So far, multisublattice dynamics is described with a Hamiltonian which takes into account the spin-spin interactions, and neglects the anisotropy due to the spin-orbit coupling [19]. This approximation is valid for Gd-TM alloys due to the small anisotropy in Gd. However, for an adequate description of the dynamics of other $4f$ rare-earth metals such as Tb, the anisotropy can not be ignored and should be included in the Hamiltonian.

Finally, element-specific probing with visible light has unique advantages compared to techniques utilizing high-energy photons [2–4], such as (i) superior signal-to-noise ratio due to the high photon flux, (ii) much less time-consuming and demanding measurements, (iii) no need for a vacuum environment, (iv) no need to work with unique sources with limited access or buy expensive tools for the generation of high-energy photons, and (v) the use of nonionizing photons. Unique advantages of XMCD measurements are the possibilities to resolve the spin and orbital angular moments [21] and to have a spatial resolution of only several nm.

In summary, we have demonstrated the feasibility of element-specific probing of ultrafast spin dynamics with (near-)visible light in a TbFe alloy. The antiferromagnetically coupled spins are brought in a transient ferromagnetic state at high excitation intensities succeeded with magnetization recovery. This is in striking contrast to GdFe, where a transient ferromagnetic state is succeeded with magnetization reversal. Furthermore, element-specific probing with visible light can be generalized to other multisublattice alloys when a single calibration with TR XMCD measurements is made.

We thank A. van Roij and A. Toonen for technical support. This research has received funding from Stichting voor Fundamenteel Onderzoek der Materie (FOM), De Nederlandse Organisatie voor Wetenschappelijk Onderzoek (NWO), and EC FP7 ITN Grant No. 214810 (FANTOMAS) and ERC Grant No. 257280 (Femtomagnetism).

*s.khorsand@science.ru.nl

[1] C. D. Stanciu, F. Hansteen, A. V. Kimel, A. Kirilyuk, A. Tsukamoto, A. Itoh, and T. Rasing, Phys. Rev. Lett. **99**, 047601 (2007).
[2] I. Radu *et al.*, Nature (London) **472**, 205 (2011).
[3] C. Stamm *et al.*, Nat. Mater. **6**, 740 (2007).
[4] C. La-O-Vorakiat, M. Siemens, M. M. Murnane, H. C. Kapteyn, P. Grychtol, R. Adam, C. M. Schneider, J. M. Shaw, H. Nembach, and T. J. Silva, Phys. Rev. Lett. **103**, 257402 (2009).
[5] E. Beaurepaire, J. C. Merle, A. Daunois, and J. Y. Bigot, Phys. Rev. Lett. **76**, 4250 (1996).
[6] B. Koopmans, M. van Kampen, J. T. Kohlhepp, and W. J. M. de Jonge, Phys. Rev. Lett. **85**, 844 (2000).
[7] B. Koopmans, G. Malinowski, F. D. Longa, D. Steiauf, M. Fähnle, T. Roth, M. Cinchetti, and M. Aeschlimann, Nat. Mater. **9**, 259 (2010).
[8] L. Guidoni, E. Beaurepaire, and J. Y. Bigot, Phys. Rev. Lett. **89**, 017401 (2002).
[9] M. Sultan, U. Atxitia, A. Melnikov, O. Chubykalo-Fesenko, and U. Bovensiepen, Phys. Rev. B **85**, 184407 (2012).
[10] P. Hansen, *Handbook of Magnetic Materials*, edited by K. Buschow (Elsevier, New York, 1991), Vol. 6.
[11] P. Hansen, C. Clausen, G. Much, M. Rosenkranz, and K. Witter, Jpn. J. Appl. Phys. **66**, 756 (1989).
[12] E. Arenholz, E. Navas, K. Starke, L. Baumgarten, and G. Kaindl, Phys. Rev. B **51**, 8211 (1995).
[13] S. Hufner, F. Schumann, E. Rotenberg, J. Tobin, S. H. Yang, B. S. Mun, S. Morton, J. Schafer, and D. Ehm, Phys. Rev. B **63**, 085106 (2001).
[14] J. K. Lang, Y. Baer, and P. A. Cox, J. Phys. F **11**, 121 (1981).
[15] K. M. Dobrich, G. Bihlmayer, K. Starke, J. E. Prieto, K. Rossnagel, H. Koh, E. Rotenberg, S. Blugel, and G. Kaindl, Phys. Rev. B **76**, 035123 (2007).
[16] M. Wietstruk, A. Melnikov, C. Stamm, T. Kachel, N. Pontius, M. Sultan, C. Gahl, M. Weinelt, H. A. Dürr, and U. Bovensiepen, Phys. Rev. Lett. **106**, 127401 (2011).
[17] See Supplemental Material at http://link.aps.org/supplemental/10.1103/PhysRevLett.110.107205 for a discussion on the feasibility of element-specific probing with visible light in any two-sublattice magnets employing a calibration of probe sensitivities with TR XMCD measurements.
[18] A. Delin, O. Eriksson, B. Johansson, S. Auluck, and J. M. Wills, Phys. Rev. B **60**, 14 105 (1999).
[19] J. H. Mentink, J. Hellsvik, D. V. Afanasiev, B. A. Ivanov, A. Kirilyuk, A. V. Kimel, O. Eriksson, M. I. Katsnelson, and T. Rasing, Phys. Rev. Lett. **108**, 057202 (2012); T. A. Ostler *et al.*, Nat. Commun. **3**, 666 (2012).
[20] A. R. Khorsand, M. Savoini, A. Kirilyuk, A. V. Kimel, A. Tsukamoto, A. Itoh, and T. Rasing, Phys. Rev. Lett. **108**, 127205 (2012).
[21] B. T. Thole, P. Carra, F. Sette, and G. van der Laan, Phys. Rev. Lett. **68**, 1943 (1992).